Editors' Suggestion

Three-dimensional topological orbital Hall effect caused by magnetic hopfions

Börge Göbel ⓘ* and Samir Lounis ⓘ

Institut für Physik, Martin-Luther-Universität Halle-Wittenberg, D-06099 Halle (Saale), Germany

Magnetic hopfions are noncollinear spin textures that are characterized by an integer topological invariant, called the Hopf index. The three-dimensional magnetic solitons can be thought of as a tube with a twisted magnetization that has been closed at both ends to form a torus. The tube consists of a magnetic whirl called an in-plane skyrmion or bimeron. Although hopfions have been observed by microscopy techniques, their detection remains challenging as they lack an electronic hallmark so far. Here we predict a three-dimensional orbital Hall effect caused by hopfion textures: When an electric field is applied, the hopfion generates a transverse current of orbital angular momentum. The effect arises due to the local emergent field that gives rise to in-plane and out-of-plane orbital Hall conductivities. This orbital Hall response can be seen as a hallmark of hopfions and allows us to distinguish them from other textures, such as skyrmioniums, that look similar in real-space microscopy experiments. While the two-dimensional topological invariant of a skyrmion determines its topological Hall transport, the unique three-dimensional topological orbital Hall effect can be identified with the three-dimensional topological invariant that is the Hopf index. Our results make hopfions attractive for spin-orbitronic applications because their orbital signatures allow for their detection in devices and give rise to large orbital torques.

I. INTRODUCTION

Noncollinear spin textures have emerged as a central topic in condensed matter physics due to their rich physics and potential applications in spintronic devices. Unlike collinear magnetic systems, where spins align uniformly in parallel or antiparallel configurations, noncollinear arrangements exhibit spatially varying spin orientations that can even give rise to topologically nontrivial spin textures, such as the family of two-dimensional magnetic whirls [1] including skyrmions [2–5], antiskyrmions [6–8], and bimerons [9–11]. These textures can be considered as solitons that can be moved by current-induced spin torques and can be easily identified by real-space microscopy imaging techniques. Their topological nature gives rise to an effective magnetic field, called emergent field [12], that causes a topological Hall effect which is a unique signature of skyrmions [13–16] and many related textures [10,17–20].

Magnetic hopfions [21–35] consist of a bimeron tube that has been twisted once and that has been merged at both ends to form a torus. These noncollinear magnetic solitons are innately three-dimensional [see Fig. 1(a)], which makes their physics even richer as they possess more degrees of freedom. For example, not only can they be moved by currents

[28,30] but they can also be tilted [29,30]. Detecting these objects remains a difficult challenge, since hopfions do not exhibit a sizable topological Hall effect [29], and typical real-space microscopy techniques rely on two-dimensional projections of the magnetic textures, which is problematic for a three-dimensional soliton: The detectable signals caused by hopfions look similar to those of a skyrmionium [19,36,37]—a skyrmion that resides at the center of another skyrmion with reversed magnetization. Still, the experimental observation of hopfions has been achieved using a combination of x-ray photoemission electron microscopy (X-PEEM) and magnetic soft x-ray transmission microscopy (MTXM) [32] or Lorentz transmission electron microscopy (LTEM) [35]. However, a more conclusive detection method would reveal the actual three-dimensional texture, which is, in principle, possible by holography or tomography techniques using x-rays or electrons [38–45]. Unfortunately, these techniques are highly demanding and not compatible with potential spintronic applications of hopfions. A simple electric or magnetic signature of hopfions is desired to make these textures usable in devices.

Therefore, we consider the research field of orbitronics, which has attracted great interest recently. It is concerned with the orbital angular momentum and the related orbital current. In equilibrium, the orbital angular momentum of a solid is often quenched because of the high symmetry, which is why the magnetization of most ferromagnets originates from the spin degree of freedom. However, when an electric field drives a system out of equilibrium, a sizable density of orbital magnetic moment or transverse orbital currents can be generated. These phenomena are called orbital Edelstein effect [46–59] and orbital Hall effect [60–75], respectively,

---

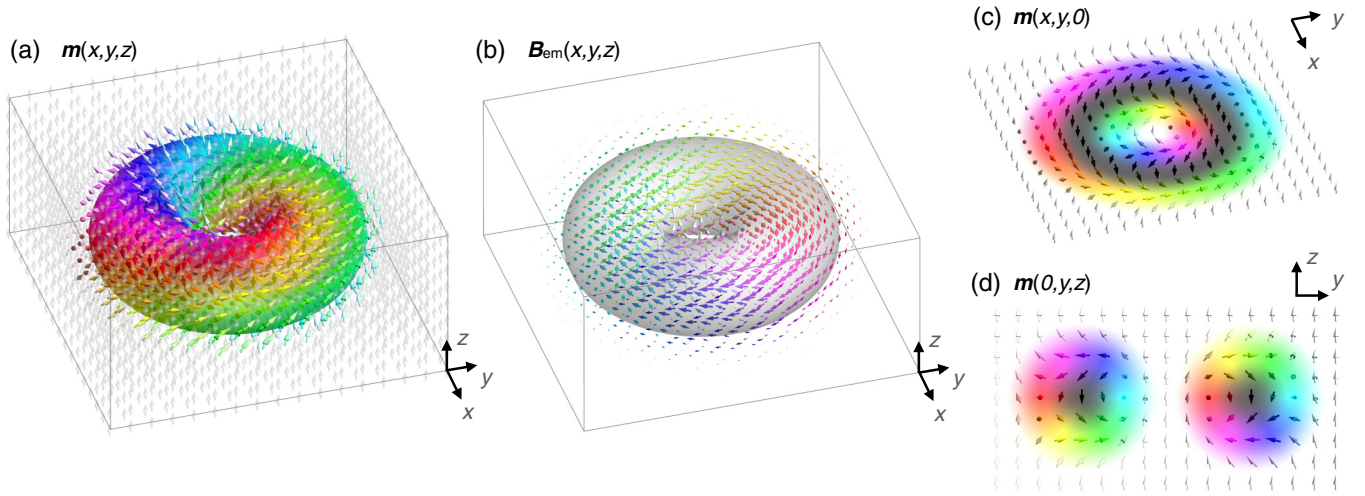*Contact author: boerge.goebel@physik.uni-halle.de

FIG. 1. Magnetic hopfion. (a) Magnetic texture $m(r)$ of a $\lambda = 8a$ hopfion. (b) Corresponding emergent field $B_{em}(r)$. (c) A cut along the xy plane reveals a magnetic skyrmionium. (d) A cut along the the yz plane reveals two in-plane skyrmions also called bimerons. The color of the arrows in all panels encodes their orientation in the xy plane. White and black arrows point along the positive and negative z directions, respectively. Note that these arrows that surround the hopfion have been plotted translucently to allow for a clearer view of the noncollinear part of the texture.

and they are often larger than their spin counterparts. The orbital effects often exist even without the relativistic spin-orbit coupling and only a small portion of these orbital signals gets converted to a spin Edelstein effect or a spin Hall effect due to this relativistic mechanism. Noncollinear spin textures with a nontrivial topology, such as the magnetic skyrmion, give rise to an orbital magnetization [76–78] in equilibrium, and have been shown to exhibit a topological orbital Hall effect once an electric field is applied [75]. Even textures with a compensated emergent field, such as antiferromagnetic skyrmions [79–82], can exhibit such an effect [75] due to the local presence of an emergent field, even though it is compensated on average.

In this paper, we use a tight-binding and Kubo approach and predict a three-dimensional topological orbital Hall effect caused by hopfion textures. This effect is generated by their local emergent field that gives rise to an orbital Berry curvature (see Fig. 2) and causes out-of-plane and in-plane orbital Hall conductivities (see Fig. 3). The orbital Hall signatures of a hopfion are unique and allow us to distinguish it from two-dimensional topological textures, such as the skyrmion, bimeron, or skyrmionium. While the two-dimensional topological invariant of a skyrmion determines its topological Hall transport, the unique three-dimensional orbital Hall transport is a manifestation of the three-dimensional topological invariant called the Hopf index. Although all results presented in this paper rely on quantum mechanical calculations, they can be understood semiclassically on the basis of the emergent field of the textures and the carrier density of the conduction electrons.

This paper is structured as follows. We begin by detailing the tight-binding method used throughout this paper. In Sec. II A we discuss the considered hopfion texture that enters the Hamiltonian and in Sec. II B we present the Kubo approach that allows us to calculate the orbital Hall conductivity. The results of these calculations are presented in Sec. III A. In Sec. III B we compare the results with the Hall transport caused by textures that are closely related to hopfions: (i)

skyrmion tubes, (ii) bimeron tubes, and (iii) skyrmionium tubes. The energy dependencies of the orbital Hall conductivities can be understood by analyzing the carrier density and the emergent magnetic field of these textures; see Sec. III C. Finally, we conclude in Sec. IV.

II. MODEL AND METHODS

Throughout this paper, we use a tight-binding model to describe the conduction electrons and their spins' interaction with the hopfion texture (Sec. II A). The orbital conductivity
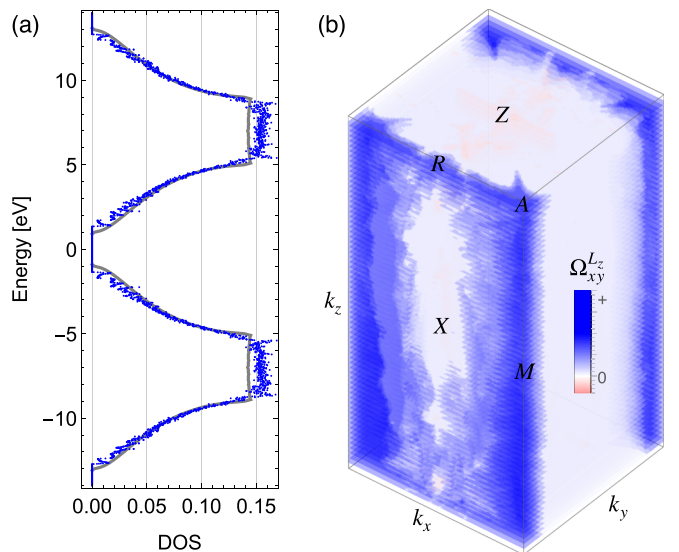

FIG. 2. Electronic properties caused by a hopfion with $m = 7t$. (a) Density of states [Eq. (9)] (blue) and comparison to the density of states without the hopfion (gray). (b) Slices of the orbital Berry curvature $\Omega_{v,xy}^{L_z}(k)$ of the lowest band $\nu = 1$.
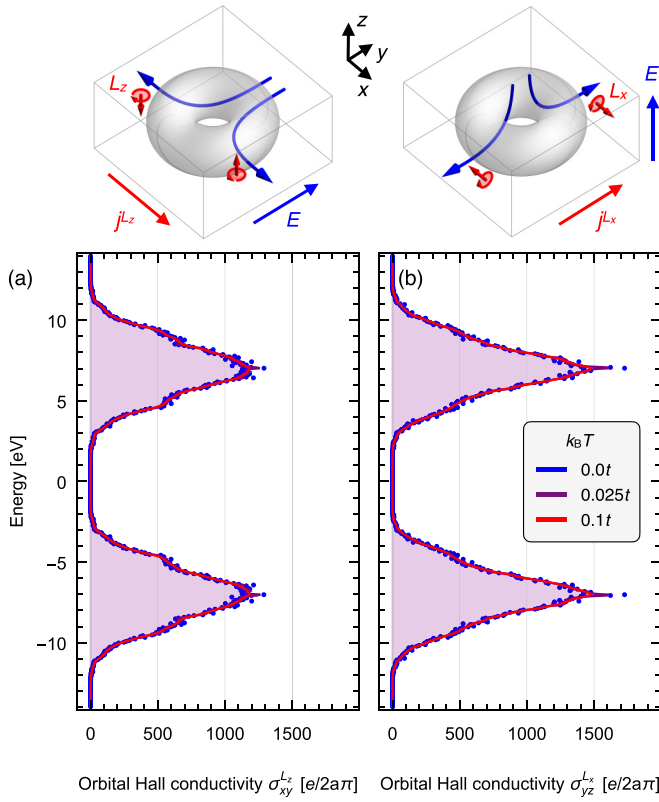
FIG. 3. Three-dimensional orbital Hall effect caused by a hopfion in the strong-coupling limit. (a) The orbital conductivity tensor element $\sigma_{xy}^{L_z}$ as a function of energy. This orbital Hall conductivity characterizes a transport of orbital angular momentum L_z in the Hopfion plane xy. Application of an electric field $\boldsymbol{E}$ along y gives rise to an orbital current $\boldsymbol{j}^{L_z}$ along x; see schematic image above. The orbital angular momentum is polarized out of plane. (b) The equivalent results for the $\sigma_{yz}^{L_x} = \sigma_{zx}^{L_y}$ tensor element. The Hund's coupling is characterized by $m = 7t$ so that the conduction electrons' spins almost completely align with the hopfion texture. The color of the curve indicates the temperature; see legend.

tensor elements are calculated based on a Kubo approach (Sec. II B).

A. Hopfion texture

First, we want to introduce the hopfion texture $\boldsymbol{m}(\boldsymbol{r})$ and discuss its topological properties. $\boldsymbol{m}$ is the normalized magnetic moment and $\boldsymbol{r}$ is the position vector. We use the top-down view coordinates x, y with $r = \sqrt{x^2 + y^2}$ the distance and $\phi = \arctan(y/x)$ the polar angle, as well as the transformed coordinates $\rho_x = r - \lambda/2$, $\rho_y = z$ with $\rho = \sqrt{\rho_x^2 + \rho_y^2}$. The hopfion is modeled as

$$\boldsymbol{m}(\boldsymbol{r}) = \begin{pmatrix} \sin(2\pi\rho/\lambda)\frac{x\rho_y - y\rho_x}{r\rho} \\ \sin(2\pi\rho/\lambda)\frac{x\rho_x + y\rho_y}{r\rho} \\ -\cos(2\pi\rho/\lambda) \end{pmatrix} \quad (1)$$

in the volume of the torus $\sqrt{(x - \lambda/2 \cdot \cos\phi)^2 + (y - \lambda/2 \cdot \sin\phi)^2 + z^2}$ $< \lambda/2$ and $\boldsymbol{m}(\boldsymbol{r}) = \boldsymbol{e}_z$ elsewhere. This texture is topologically equivalent to the ones used in the literature, e.g., Refs. [25,29],

but has a homogeneous background. This is important because the orbital Hall transport will be calculated based on a reciprocal-space approach, so we need periodicity in real space. The texture above describes the texture in a unit cell of size $2\lambda \times 2\lambda \times \lambda$.

The hopfion texture is shown in Fig. 1(a) and can be thought of as a skyrmion tube that is magnetized in the plane of the tube, has been twisted once, and whose ends have been merged to form a torus. In our calculations, the torus is located in the xy plane. If the three-dimensional magnetic texture is cut along the xy plane, the result is a skyrmionium: a skyrmion that is positioned at the center of another skyrmion with opposite magnetization. This cut containing the skyrmionium is shown in Fig. 1(c). If one cuts the hopfion along a plane that contains the z axis, e.g., the yz plane, one can see the texture of the skyrmion tube that forms the hopfion. However, as explained before, it is actually an in-plane magnetized skyrmion, which is called bimeron, and, since the torus is cut twice by the plane, we see two bimerons in Fig. 1(d). In Sec. III B we will show that the orbital Hall response of a hopfion is related to the orbital Hall responses of these two-dimensional textures.

An explanation will be provided on the basis of the emergent field of a magnetic texture, which is a quantity that determines its topological Hall transport and orbital Hall transport. Its $\alpha = x, y, z$ component is defined as [12]

$$B_{em,\alpha}(\boldsymbol{r}) = \frac{1}{2}\sum_{\beta,\gamma}\epsilon_{\alpha\beta\gamma}\,\boldsymbol{m}(\boldsymbol{r})\cdot\left(\frac{\partial\boldsymbol{m}(\boldsymbol{r})}{\partial\beta}\times\frac{\partial\boldsymbol{m}(\boldsymbol{r})}{\partial\gamma}\right). \quad (2)$$

The emergent field of a hopfion is shown in Fig. 1(b). Unlike the case of two-dimensional textures discussed before, it is noncollinear and has a toroidal configuration in the hopfion torus. In the center of the hopfion it points out of the torus plane. On average, the emergent field of the hopfion is compensated.

Two-dimensional topological textures, such as magnetic skyrmions, bimerons and skyrmioniums that constitute cuts of the hopfion are characterized by the topological charge

$$N_{Sk} = \frac{1}{4\pi}\int\boldsymbol{m}(\boldsymbol{r})\cdot\left(\frac{\partial\boldsymbol{m}(\boldsymbol{r})}{\partial\beta}\times\frac{\partial\boldsymbol{m}(\boldsymbol{r})}{\partial\gamma}\right)d^2r. \quad (3)$$

Here we have assumed that the texture changes in the $\beta\gamma$ plane and is constant along α. In this case, the topological charge N_{Sk} is the integral of the perpendicular emergent field $B_{em,\alpha}(\boldsymbol{r})$ over the whole texture. While a skyrmion and a bimeron tube are characterized by a nontrivial topological invariant $N_{Sk} = \pm 1$, the two-dimensional cuts through the hopfion always contain two skyrmions or two bimerons with opposite topological charges. Therefore, the skyrmionium in Fig. 1(c) and the pair of bimerons in Fig. 1(d) are topologically trivial, $N_{Sk} = 0$.

A hopfion is a three-dimensional texture. Therefore, it is not reasonable to characterize it by the topological charge N_{Sk} as defined above. Still, the emergent field is important to characterize its topology. A hopfion is characterized by the Hopf index [83–85]

$$N_H = -\frac{1}{(4\pi)^2}\int\boldsymbol{B}_{em}(\boldsymbol{r})\cdot\boldsymbol{A}(\boldsymbol{r})d^3r. \quad (4)$$

It is $N_H = \pm 1$ depending on the type of hopfion and is calculated from the emergent field $\boldsymbol{B}_{\mathrm{em}}(\boldsymbol{r})$ and the corresponding vector potential $\boldsymbol{A}(\boldsymbol{r})$. Like every vector potential it is not gauge invariant and fulfills $\nabla \times \boldsymbol{A} = \boldsymbol{B}_{\mathrm{em}}$. The emergent field and the Hopf index are gauge invariant. So far, the role of the Hopf index has only been discussed in terms of topological stability of the hopfion but not in terms of transport properties. This is the purpose of this work as we identify the unique orbital Hall response caused by hopfions.

Although the textures as defined throughout this section are continuous functions of the position vector $\boldsymbol{r}$, for the tight-binding calculations we consider a discrete lattice. Therefore, the texture $\boldsymbol{m}(\boldsymbol{r})$ is rather a set of magnetic moments $\{\boldsymbol{m}_i\}_{i=1,\ldots,N}$ that are defined at the sites $\{\boldsymbol{r}_i\}_{i=1,\ldots,N}$. Since the calculation of a three-dimensional magnetic texture is computationally demanding, we are restricted when choosing appropriate hopfion sizes for the calculations. Here we use a unit cell consisting of $N = 256$ magnetic moments, which is enough to capture the topological properties of the hopfion as well as of the skyrmionium and bimerons accurately.

B. Calculation of Hall conductivities

The electronic Hamiltonian is based on a tight-binding approach and is written here in second quantization [75,86–89]:

$$H = -t \sum_{\langle ij \rangle} c_i^\dagger c_j + m \sum_i \boldsymbol{m}_i \cdot (c_i^\dagger \boldsymbol{\sigma} c_i). \qquad (5)$$

$c_i^\dagger$ and c_i are the creation and annihilation operators of an s electron at site i. $\boldsymbol{\sigma}$ is the vector of Pauli matrices. The Hamiltonian has the dimension $2N \times 2N$.

The first term describes the kinetic energy of the conduction electrons via hopping terms of the form $-t \exp[i\boldsymbol{k} \cdot (\boldsymbol{r}_i - \boldsymbol{r}_j)]$. Here, $\boldsymbol{k}$ is the wave vector and $\boldsymbol{r}_i - \boldsymbol{r}_j$ the hopping path. For the hopping amplitude we choose $t = 1$ eV and for the lattice constant $a = 2.76$ Å. We consider a three-dimensional cubic lattice. The second term describes the coupling of the conduction electrons with the magnetic texture $\{\boldsymbol{m}_i\}$ that is formed by energetically lower states, e.g., by d electrons. Throughout this paper, we consider two cases: (i) the adiabatic limit, where the conduction electrons' spins align almost perfectly with the texture (here $m = 7t$), and the weak-coupling case, where spin parallel and antiparallel states are hybridized (here $m = 2t$).

Equation (5) is the so-called sd Hamiltonian in which only s electrons are considered explicitly and d electrons enter only via their magnetic texture $\{\boldsymbol{m}_i\}$. This Hamiltonian is suitable for analyzing topological transport phenomena [75,86–89] and has the advantage that spin-orbit coupling is zero, so that the pure topological influence of the magnetic texture on the Hall conductivities can be calculated. Note that spin-orbit coupling is not required for the emergence of a topological Hall effect, topological orbital Hall effect, or topological spin Hall effect [75].

We diagonalize the sd Hamiltonian to numerically determine its eigensystem. The eigenvalues $E_{\nu k}$ constitute the band structure with band index $\nu = 1, \ldots, 2N$. From the eigenvectors $|\nu k\rangle$ we calculate the Hall conductivities. The orbital Hall transport is quantified by the orbital Hall conductivity [66]

$$\sigma_{xy}^{L_z}(E_{\mathrm{F}}) = \frac{e}{\hbar} \sum_\nu \frac{1}{(2\pi)^3} \int_{E_{\nu k} \leqslant E_{\mathrm{F}}} \Omega_{\nu,xy}^{L_z}(\boldsymbol{k}) \, \mathrm{d}^3 k. \qquad (6)$$

This equation assumes temperature $T = 0$ and is a function of the Fermi energy E_{F}. We integrate over the orbital Berry curvature

$$\Omega_{\nu,xy}^{L_z}(\boldsymbol{k}) = -2\hbar^2 \, \mathrm{Im} \sum_{\mu \neq \nu} \frac{\langle \nu \boldsymbol{k}| j_x^{L_z} |\mu \boldsymbol{k}\rangle \langle \mu \boldsymbol{k}|v_y|\nu \boldsymbol{k}\rangle}{(E_{\nu k} - E_{\mu k})^2}. \qquad (7)$$

Although the electronic transport is determined by all occupied states, the influence of the d electrons is negligible because they are fully occupied and far away from the s states near the Fermi level. For calculating the orbital Hall conductivity at finite temperatures $T > 0$, the orbital Berry curvature is weighted by the Fermi-Dirac distribution function in the energy integral.

We use the velocity operator $v_l = \frac{1}{\hbar} \frac{\partial H}{\partial k_l}$ and the orbital current operator $\langle \nu \boldsymbol{k}| j_x^{L_z} |\mu \boldsymbol{k}\rangle = \frac{1}{2} \sum_\alpha [\langle \nu \boldsymbol{k}|v_x|\alpha \boldsymbol{k}\rangle \langle \alpha \boldsymbol{k}|L_z|\mu \boldsymbol{k}\rangle + \langle \nu \boldsymbol{k}|L_z|\alpha \boldsymbol{k}\rangle \langle \alpha \boldsymbol{k}|v_x|\mu \boldsymbol{k}\rangle]$. The orbital angular momentum $\langle \nu \boldsymbol{k}|L_z|\alpha \boldsymbol{k}\rangle$

$$\begin{aligned} &= i\frac{e\hbar^2}{4g_L\mu_{\mathrm{B}}} \sum_{\beta \neq \nu,\alpha} \left(\frac{1}{E_{\beta k} - E_{\nu k}} + \frac{1}{E_{\beta k} - E_{\alpha k}} \right) \\ &\quad \times \left(\langle \nu \boldsymbol{k}|v_x|\beta \boldsymbol{k}\rangle \langle \beta \boldsymbol{k}|v_y|\alpha \boldsymbol{k}\rangle - \langle \nu \boldsymbol{k}|v_y|\beta \boldsymbol{k}\rangle \langle \beta \boldsymbol{k}|v_x|\alpha \boldsymbol{k}\rangle \right) \end{aligned} \qquad (8)$$

has been calculated based on the modern formulation [90–95] and takes into account intersite contributions [66] that are not considered in the often used atomic-center approximation. Using this more accurate description has been shown to be of crucial importance for topologically nontrivial spin textures such as skyrmions, as the orbital angular momentum and the corresponding orbital Hall conductivity are caused by large cyclotron orbits generated by the texture's emergent magnetic field [75].

Although the focus of this paper is on orbital transport, we also briefly mention the topological Hall conductivity and spin Hall conductivity, as defined in Ref. [75].

III. RESULTS AND DISCUSSION

Next, we present the results of our calculations and begin with the orbital Hall signatures of hopfions in Sec. III A. Afterwards, in Sec. III B, we compare them with the typical Hall signatures of related noncollinear textures: (i) skyrmion tubes, (ii) bimeron tubes, and (iii) skyrmionium tubes. In Sec. III C, we present how the energy dependence of the orbital Hall conductivities can be understood by analyzing the carrier density and the emergent field of these textures.

A. Orbital Hall transport of hopfions

Diagonalizing the Hamiltonian [Eq. (5)] and using the hopfion texture [Eq. (1)] results in the band structure describing electrons interacting with a periodic array of hopfions. In the strong-coupling case, where $m = 7t$, the band structure exhibits two blocks consisting of 256 bands each. The conduction electron spins align locally parallel and antiparallel with

the hopfion texture in the two blocks, respectively. The blocks are centered around $\pm m$ and have a band width of almost $12t$. Due to the large number of bands, it is not helpful to look at the band structure directly, as the bands are very dense.

1. Density of states

Instead, the density of states, shown in Fig. 2(a) for the strong-coupling case $m = 7t$, reveals better how the states are distributed in energy. This function quantifies the states in an energy interval around E:

$$\mathrm{DOS}(E) = \frac{1}{(2\pi)^3} \sum_\nu \int \delta(E - E_{\nu\mathbf{k}})\, \mathrm{d}^3 k. \qquad (9)$$

Near the band edges, we see an increase and a rather constant plateau near the centers of the blocks around $\pm m$. The density of states (blue) agrees rather well with the density of states of the band structure that characterizes the underlying square lattice (gray). It consists of two bands that we have shifted by $\pm m$

$$E_{3\mathrm{D}}(\mathbf{k}) = -2t[\cos(k_x a) + \cos(k_y a) + \cos(k_z a)] \pm m. \quad (10)$$

Due to the topological properties of the hopfion texture, an emergent field arises that acts just like an actual magnetic field that couples to the charge of the electrons. For a two-dimensional system, like a thin sample hosting skyrmions, it leads to the emergence of Landau levels whose energy is determined by the density of states [96] according to Onsager's quantization scheme [97]. Even though here the discussion is more difficult, due to the three-dimensional nature of the system and the globally compensated emergent field, we still find that the density of states of the magnetic system (hosting a hopfion) and the nonmagnetic system (characterized by $E_{3\mathrm{D}}(\mathbf{k})$) are relatable.

In summary, the band structure exhibits a dense collection of bands whose density of states agrees well with the density of states of the nonmagnetic system. The two cosine-shaped bands of the cubic lattice condense to many rather flat bands because of the emergent field of the hopfion. Next, we analyze the orbital Hall conductivity that is determined by the eigenvectors that are affected by the emergent field as well.

2. Orbital Hall transport

The bands exhibit nonvanishing orbital angular momenta that have been calculated based on the modern formulation of orbital magnetization [Eq. (8)]. Also, the hopfion gives rise to a net orbital Berry curvature [shown in Fig. 2(b) for the strong-coupling case $m = 7t$] that causes an orbital Hall conductivity; see Fig. 3. Interestingly, since the emergent field [Fig. 1(b)] has components in all directions in space, not only the orbital Hall tensor elements $\sigma_{xy}^{L_z} = -\sigma_{yx}^{L_z}$ [presented in Fig. 3(a)] are nonzero but also the elements $\sigma_{yz}^{L_x} = -\sigma_{zy}^{L_x} = \sigma_{zx}^{L_y} = -\sigma_{xz}^{L_y}$ [presented in Fig. 3(b)]. This is unlike the orbital Hall effect of any two-dimensional texture in the xy plane, which can only exhibit the orbital Hall conductivity $\sigma_{xy}^{L_z} = -\sigma_{yx}^{L_z}$, as discussed in more detail in Sec. III B. Therefore, we call this unique signature of the hopfion the three-dimensional orbital Hall effect.
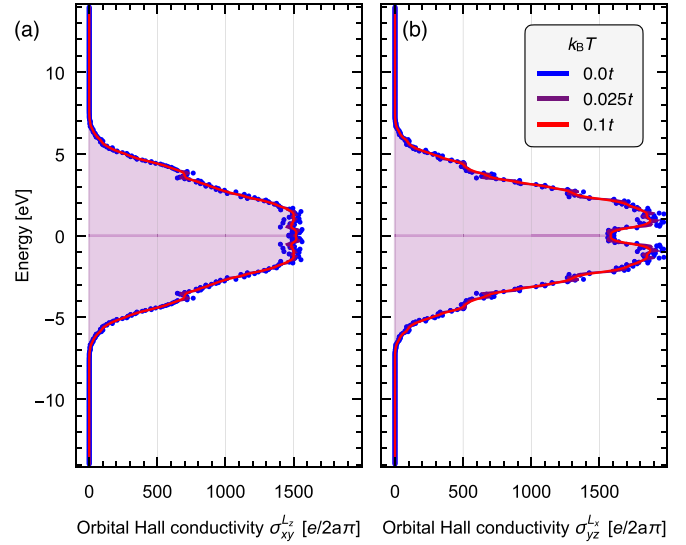

FIG. 4. Three-dimensional orbital Hall effect caused by a hopfion in the weak-coupling limit. The figure is analogous to Fig. 3 but with a weaker Hund's coupling of $m = 2t$. (a) The orbital conductivity tensor element $\sigma_{xy}^{L_z}$ and (b) the tensor element $\sigma_{yz}^{L_x} = \sigma_{zx}^{L_y}$ are shown as a function of energy for various temperatures.

The presence of an orbital Hall effect is not related to the finite size of the hopfion but can be expected even for a perfectly smooth texture because the orbital Hall conductivity is known to be insensitive to the sign of the emergent field [75]. For this reason, any texture with an emergent field can give rise to an orbital Hall effect even if it is compensated on average. We recently demonstrated this for an antiferromagnetic skyrmion which consists of two sublattices with opposite emergent fields. These opposite fields cause the same orbital Hall conductivity because they give rise to opposite orbital angular momenta and opposite charge Hall transport [75].

The energy-dependent curves in Figs. 3(a) and 3(b) look rather similar for both tensor components except for a difference in magnitude. Furthermore, they are almost identical for the upper and lower blocks in energy and the signal is symmetric within each block, starting at zero near the band edges and exhibiting a maximum near the center of each block. A detailed analysis of the energy dependence of these orbital conductivities and their relation to the emergent field follows later in Sec. III C. The magnitude of the orbital Hall conductivity scales with the component of $1/\langle B_{\mathrm{em},\alpha}^2 \rangle$ that is perpendicular to the plane of transport. Here, the brackets indicate an average over the whole hopfion. The hopfion has a larger out-of-plane component $\langle B_{\mathrm{em},z}^2 \rangle$ than the in-plane components $\langle B_{\mathrm{em},x}^2 \rangle = \langle B_{\mathrm{em},y}^2 \rangle$, which is why $\sigma_{yz}^{L_x}$ [presented in Fig. 3(b)] is larger than $\sigma_{xy}^{L_z}$ [presented in Fig. 3(a)] with maximum value of $\sim 1500\, \frac{e}{2a\pi}$ and $\sim 1200\, \frac{e}{2a\pi}$, respectively.

The orbital Hall conductivity for the weak-coupling case, $m = 2t$, is shown in Fig. 4. We see the same tensor components as before but there is no longer a separation into two blocks. Instead, spin parallel and antiparallel states that feel opposite emergent fields are hybridized. However, since opposite emergent fields result in the same orbital Hall response, this still leads to a considerable orbital Hall effect,

even in the weak-coupling limit. In fact, for some energies, the orbital Hall conductivity is even larger for $m = 2t$ than in the strong coupling case $m = 7t$. This is because the density of states is larger when there is no formation of two separate spin-polarized blocks in the band structure.

When comparing the in-plane orbital Hall conductivity $\sigma_{xy}^{L_z}$ in Fig. 4(a) with the out-of-plane orbital Hall conductivity $\sigma_{yz}^{L_x}$ in Fig. 4(b), we see similar energy dependencies but different peak structures near $E = 0$. For a smooth and infinitely large texture with a homogeneous emergent field, we would expect qualitatively equal curves. However, because of the finite size of the hopfion, differences occur near the center of the energy range. Here electronlike spin parallel states hybridize with holelike spin antiparallel states, which is why small changes or inhomogeneities in the emergent field can lead to quite strong changes in the orbital Hall conductivities.

So far, we have discussed only one type of hopfion. We have repeated our calculations from the strong-coupling limit, $m = 7t$ presented in Fig. 3, for different types of hopfions. By reversing m_z, the Hopf index and the emergent field change sign. As a consequence, the band structure changes $E_\nu(k_x, k_y, k_z) \to E_\nu(k_x, k_y, -k_z)$. However, all orbital Hall conductivity tensor elements remain unaffected by the change of the Hopf index. The same happens when we reverse an in-plane component, say m_x, instead. Due to the opposite winding, the Hopf index and the emergent field change sign but the orbital Hall conductivity is unaffected. This fits well the explanation that the orbital Hall conductivity is caused by the square of the emergent field, which is not sign sensitive. We will elaborate on this explanation in more detail in Sec. III C.

Before we continue, we would like to note that the bands also exhibit a finite Berry curvature and spin Berry curvature that give rise to a small topological Hall effect and spin Hall effect, respectively. A smooth hopfion texture has a globally compensated emergent field and so these effects are not expected. In our calculations, they occur because of the finite size of the hopfion that is limited by the computation time. The hopfion texture is not exactly smooth, which is why we find a finite topological Hall and spin Hall conductivity near the band edges. However, these signals are weak when we compare them to other textures such as skyrmion tubes; see Sec. III B. The effects would disappear for larger hopfion sizes $\lambda/a \to \infty$.

B. Comparison with related noncollinear textures

Before we examine the origin of the orbital Hall effect in more detail, first we want to compare our calculations with those for related noncollinear spin textures: (i) skyrmion tubes, (ii) bimeron tubes, and (iii) skyrmionium tubes. We analyze their orbital Hall conductivities because a hopfion can be understood as a bimeron tube that has been twisted and closed to form a torus. This bimeron tube is topologically equivalent to a skyrmion tube, because a bimeron is essentially a skyrmion in an in-plane magnet. For this reason, cutting a hopfion along a plane containing the z axis results in two bimerons; see Fig. 1(d). When a hopfion is cut along the xy plane instead, the resulting texture is a skyrmionium; see Fig. 1(c). Therefore, the results for the bimeron and for the

skyrmionium tube will help us to better understand the orbital Hall signatures of the hopfion.

1. Skyrmion tube

The first comparison with a two-dimensional texture that comes to mind is to relate our findings to the orbital Hall response of a skyrmion tube. This texture [Fig. 5(a)] exhibits a topologically nontrivial configuration in the two-dimensional xy plane that is continued along the z direction. The corresponding emergent field [Fig. 5(b)] is collinear and points along z because the texture only changes along the xy plane.

We find a sizable $\sigma_{xy}^{L_z} = -\sigma_{yx}^{L_z}$ orbital conductivity tensor element [Fig. 5(c) for the strong coupling case $m = 7t$] that exhibits an energy dependence similar to that for the hopfion; see with Fig. 3(a). The maximum is smaller with $\sim 650 \, \frac{e}{2a\pi}$ which is due to the larger emergent field component $\langle B_{em,z}^2 \rangle$ compared to the hopfion. The tensor elements $\sigma_{yz}^{L_x}$, $\sigma_{zy}^{L_x}$, $\sigma_{zx}^{L_y}$, and $\sigma_{xz}^{L_y}$ that were all finite for the hopfion are now zero due to $\langle B_{em,x}^2 \rangle = \langle B_{em,y}^2 \rangle = 0$. Instead, we find a nonzero topological Hall conductivity $\sigma_{xy} = -\sigma_{yx}$, presented in Fig. 5(d), that was negligible for the hopfion. This is because the topolgical Hall effect scales with the average emergent field and $\langle B_{em,z} \rangle$ is finite for the skyrmion while it is compensated for the hopfion.

The emergent field gives rise to Landau levels that cause a topological Hall effect and also an orbital Hall effect, as shown previously for a skyrmion system [75] in analogy to a quantum Hall system [74]. We analyzed the Hall conductivities of a skyrmion texture in Ref. [75] but in a two-dimensional system. The results presented in Fig. 5 differ from these because here we consider skyrmion tubes that extend infinitely along the z direction. Landau levels that are rather flat in the $k_x k_y$ plane have dispersion along the k_z direction because of the hopping of electrons along the skyrmion tube direction. This leads, for example, to the different band width and the missing quantization in the topological Hall conductivity in Fig. 5(d) in comparison to Ref. [75].

In summary, a skyrmion tube exhibits an orbital Hall conductivity $\sigma_{xy}^{L_z}$ similar to that of a hopfion, but a hopfion exhibits an additional $\sigma_{yz}^{L_x}$ and $\sigma_{zx}^{L_y}$ orbital Hall conductivity. A skyrmion on the other side exhibits a sizable topological Hall response in the σ_{xy} tensor element, which is negligible for hopfions. Therefore, skyrmions and hopfions can be nicely distinguished in transport experiments.

2. Bimeron tube

The cross section of the hopfion torus consists of two in-plane skyrmions, also called bimerons. In fact, a hopfion is just a bimeron tube that has been twisted and closed to form a torus. Furthermore, a bimeron is topologically equivalent to a skyrmion, so it is natural to analyze the Hall transport of bimerons tubes next. The tube is chosen to extend along x to resemble one of the torus plane directions.

The orbital Hall conductivity $\sigma_{yz}^{L_x}$ is shown in Fig. 6(b) as a function of energy. It is exactly the same as the orbital Hall conductivity $\sigma_{xy}^{L_z}$ of a skyrmion tube that is shown in Fig. 5(c) and was discussed before. The reason is that we have constructed the bimeron such that it has the same profile as the skyrmion. The two textures can be transformed from
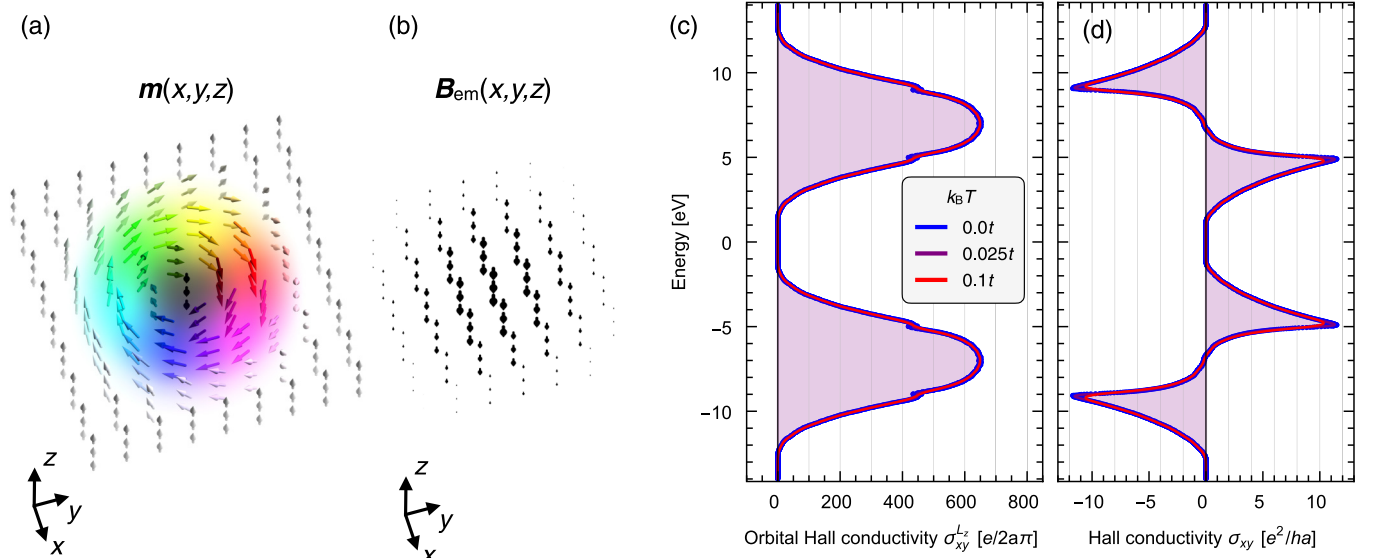
FIG. 5. Orbital Hall effect and topological Hall effect caused by a skyrmion tube. (a) Magnetic texture of the skyrmion tube. The color indicates the orientation of the magnetic moments as in Fig. 1. (b) Corresponding emergent field that is collinear and points along the tube direction. (c) Orbital Hall conductivity $\sigma_{xy}^{L_z}$ as a function of energy. (d) Topological Hall conductivity σ_{xy} as a function of energy. The color of the curve indicates the temperature; see legend. The Hund's coupling is characterized by $m = 7t$.

one to another by spin rotations of 90°. Since the emergent field is invariant under collective spin rotations, bimerons and skyrmions exhibit the same emergent field. The only difference is that we have constructed the tubes along different directions (z for the skyrmion and x for the bimeron), which is why the two textures exhibit different orbital conductivity tensor elements.

Any cross section of a hopfion that contains the z axis consists of two bimerons with opposite emergent fields. As we have shown now, such bimerons give rise to an orbital Hall conductivity along the bimeron plane. The response is the same for both bimerons, as the orbital Hall effect is insensitive to the sign of the emergent field. Each bimeron also exhibits a topological Hall conductivity σ_{yz}. However, it is exactly opposite for the two bimerons and cancels in total due to the opposite emergent fields.

In summary, a pair of oppositely magnetized bimeron tubes exhibits only an orbital Hall effect in the plane perpendicular to the tube direction. This explains why a hopfion exhibits orbital conductivity tensor elements $\sigma_{yz}^{L_x}$, $\sigma_{zy}^{L_x}$, $\sigma_{zx}^{L_y}$, and $\sigma_{xz}^{L_y}$ and why it does not exhibit a sizable topological Hall effect along these planes. Even the energy dependencies of the orbital Hall conductivities exhibit a similar shape [see Fig. 3(b) and Fig. 6(b)] but with a different maximum due to the different average emergent field $\langle B_{\text{em},x}^2 \rangle$ and $\langle B_{\text{em},y}^2 \rangle$ of the two textures.

3. Skyrmionium tube

If a hopfion is cut horizontally, the resulting texture is a skyrmionium. This two-dimensional texture consists of a skyrmion that is positioned at the center of another skyrmion with opposite topological charge. The total topological charge is compensated and therefore the average emergent field is zero. However, since the two subskyrmions exhibit out-of-plane emergent fields, a skyrmionium exhibits an average

$\langle B_{\text{em},z}^2 \rangle$. Here we consider a skyrmionium tube where the two-dimensional skyrmionium texture has been extended trivially along the z direction.

The skyrmionium tube exhibits an orbital Hall conductivity $\sigma_{xy}^{L_z}$ that is shown in Fig. 6(a). Due to the small size of the skyrmionium and the inhomogeneity of the emergent field, the curve is more noisy but in general has an energy dependence similar to that of all orbital Hall conductivities discussed before. This result for the skyrmionium allows us to understand why the hopfion exhibits an orbital Hall conductivity tensor element $\sigma_{xy}^{L_z}$; see Fig. 3(a). Both the skyrmionium and the hopfion do not exhibit a sizable topological Hall conductivity σ_{xy} due to the compensated emergent field, on average.

4. Summary

In summary, the three-dimensional orbital Hall response of a hopfion can be understood by analyzing the two-dimensional textures that appear when the hopfion is cut along a two-dimensional plane: A cut along the xy plane reveals a skyrmionium that exhibits only an orbital Hall conductivity $\sigma_{xy}^{L_z}$ and no corresponding topological Hall conductivity. A cut along the yz plane reveals a pair of bimerons that only give rise to an orbital Hall conductivity $\sigma_{yz}^{L_x}$ and not to a corresponding topological Hall conductivity. An equivalent result for $\sigma_{zx}^{L_y}$ can be found for the pair of bimerons that appear when cutting the hopfion along the zx plane.

C. Approximating the orbital Hall conductivities

As discussed in the previous sections, all nonzero orbital Hall conductivities of the various textures exhibit a similar energy dependence only with different magnitudes. The magnitude of $\sigma_{\beta\gamma}^{L_\alpha}$ is determined by the average emergent field component squared $\langle B_{\text{em},\alpha}^2 \rangle$. This is because the emergent
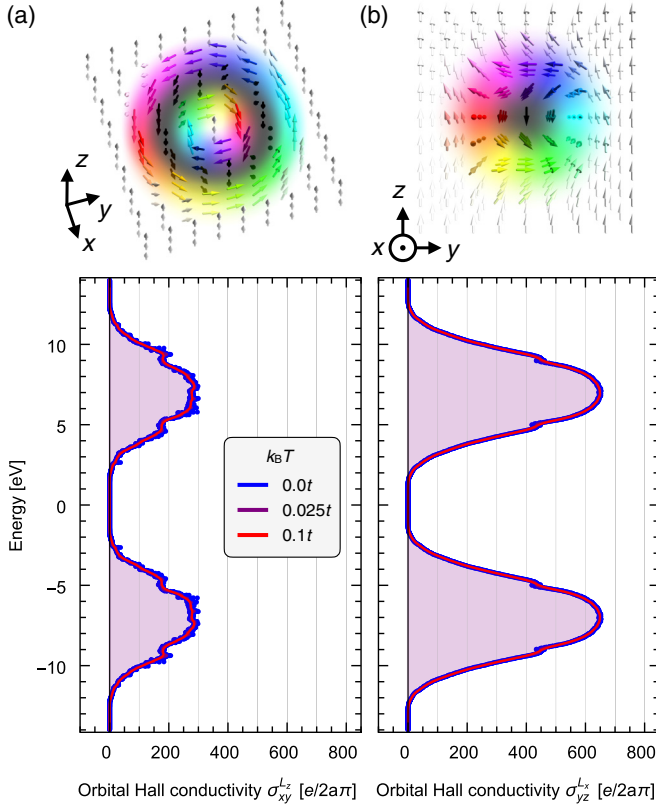
FIG. 6. Orbital Hall effect caused by two-dimensional textures related to a hopfion. (a) Top: Magnetic texture of a magnetic skyrmionium tube. The color indicates the orientation of the magnetic moments as in Fig. 1. Bottom: Orbital Hall conductivity $\sigma_{xy}^{L_z}$ as a function of energy. The color of the curve indicates the temperature; see legend. (b) Calculations for a magnetic bimeron tube. Here, the tensor element $\sigma_{yz}^{L_x}$ is nonzero. The Hund's coupling is characterized by $m = 7t$.

field causes the transverse transport of electronic states and also causes their orbital polarization. In a two-current model, oppositely orbital polarized states move along opposite directions and give rise to a net orbital current that is independent of the sign of the emergent field.

The recurring energy dependence is determined by the band structure of the underlying cubic lattice. We have already briefly identified the role of this band structure for the distribution of the electronic states in energy by discussing the density of states in Sec. III A and we will do so in more detail in the following.

As we have established in a previous work on magnetic skyrmions [75], the energy dependencies of the charge, spin, and orbital Hall conductivities can be approximated by the density of states $n'_{dD}(E) = \frac{1}{(2\pi)^d} \int \delta(E - E_{dD}(\boldsymbol{k})) \, \mathrm{d}^d k$ and the carrier density $n_{dD}(E) = \kappa(E) \int^E n'_{dD}(E') \, \mathrm{d}E'$ calculated from the band structure of the underlying lattice $E_{dD}(\boldsymbol{k})$. Here, $\kappa(E) = \pm 1$ is determined by the electronic character of the Fermi line: electronlike $(+1)$ vs holelike (-1). In that reference, a two-dimensional system, $d = 2$, in the xy plane with an emergent field along z was considered, and we found that

the orbital Hall conductivity can be approximated as

$$\sigma_{xy,\text{approx,2D}}^{L_z}(E) \propto \frac{[n_{2D}(E)]^2}{n'_{2D}(E)} \frac{1}{\langle B_{\text{em},z}^2 \rangle}. \quad (11)$$

Here, we generalize these findings of the two-dimensional system to explain the results of three-dimensional systems, $d = 3$, that were shown in Sec. III A. As an example, we discuss $\sigma_{xy}^{L_z}$ that is determined by $\langle B_{\text{em},z}^2 \rangle$. The other tensor elements can be calculated analogously by rotating the coordinate system.

When transitioning from the two-dimensional system to the three-dimensional system, the band structure of the underlying lattice changes from $E_{2D}(k_x, k_y) = -2t[\cos(k_x a) + \cos(k_y a)]$ to $E_{3D}(k_x, k_y, k_z) = -2t[\cos(k_x a) + \cos(k_y a) + \cos(k_z a)]$, so in this particular case $E_{3D}(k_x, k_y, k_z) = E_{2D}(k_x, k_y) - 2t \cos(k_z a)$. However, because the transverse transport occurs in the plane perpendicular to $\boldsymbol{B}_{\text{em}}$ (here the xy plane), we cannot simply replace the density of states and carrier density of the two-dimensional system with those of the three-dimensional system. Instead, we consider a modified density of states, the k_z-resolved density of states

$$n'(E, k_z) = \frac{1}{(2\pi)^3} \int \delta(E - E_{3D}(k_x, k_y, k_z)) \, \mathrm{d}k_x \mathrm{d}k_y \quad (12)$$

and carrier density

$$n(E, k_z) = \kappa(E, k_z) \int^E n'(E', k_z) \, \mathrm{d}E', \quad (13)$$

and integrate over the $\boldsymbol{k}$ direction along $\boldsymbol{B}_{\text{em}}$ (here along k_z). The resulting orbital Hall conductivity

$$\sigma_{xy,\text{approx,3D}}^{L_z}(E) \propto \frac{1}{\langle B_{\text{em},z}^2 \rangle} \int \frac{[n(E, k_z)]^2}{n'(E, k_z)} \, \mathrm{d}k_z \quad (14)$$

is shown in Fig. 7(a) and resembles the previously calculated orbital Hall conductivities of the various noncollinear magnetic textures well; see Figs. 3(a), 3(b), 5(c), 6(a), and 6(b).

The results of the full quantum-mechanical calculations are especially well reproduced for the skyrmion tube and the bimeron tube; see Figs. 5(c) and 6(b). For these textures, the emergent field is rather smooth and does not change along the tube direction, so that the assumptions of the approximation are well fulfilled: The electronic states are distributed according to the density of states of the underlying lattice and the orbital Berry curvature does not change much along the $\boldsymbol{k}$ direction that is along the direction perpendicular to the Hall transport. As another example, the hopfion's $\sigma_{xy}^{L_z}$ component [Fig. 3(a)] is also nicely approximated but there are small deviations. These occur because the emergent field is less smooth [Fig. 1(b)] and the orbital Berry curvature $\Omega_{xy}^{L_z}$ varies slightly along k_z [Fig. 2(b)].

Overall, we have achieved a good semiclassical understanding of the orbital Hall effect in these three-dimensional systems. The magnitude of $\sigma_{\beta\gamma}^{L_\alpha}$ is determined by the average emergent field $\langle B_{\text{em},\alpha}^2 \rangle$ and the energy dependence can be reconstructed based on the zero-field band structure of the underlying lattice $E_{3D}(\boldsymbol{k})$. For the textures with a finite topological charge N_{Sk} (in this paper the skyrmion tube and the
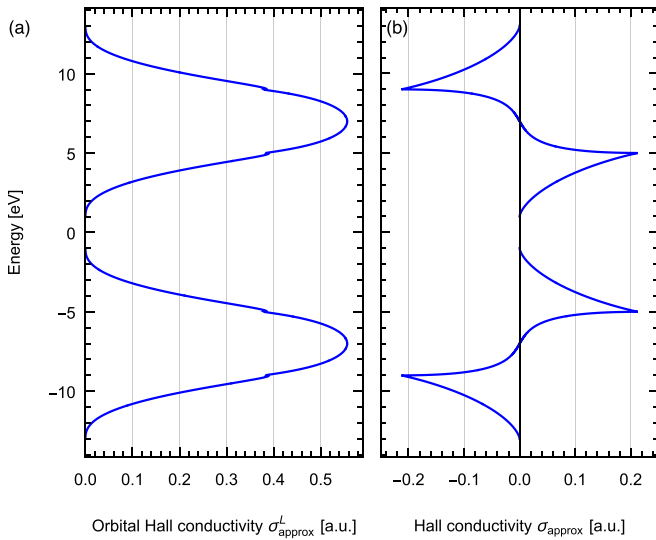
FIG. 7. Approximation of energy-dependent Hall conductivities for textures with a finite emergent field in the strong-coupling limit. (a) Orbital Hall conductivity $\sigma^L_{\mathrm{approx}}$ with the orbital angular momentum L along the emergent field and the electric field and the transverse orbital current in the plane perpendicular to it. (b) Topological Hall conductivity σ_{approx} in the plane perpendicular to the emergent field. The Hund's coupling is $m = 7t$ so that the conduction electrons' spins can be assumed to align with the magnetic texture.

bimeron tube), we can also approximate the topolgical Hall conductivity and the spin Hall conductivity as

$$\sigma_{xy,\mathrm{approx,3D}}(E) \propto \pm \frac{1}{\langle B_{\mathrm{em},z}\rangle}\int n(E,k_z)\,\mathrm{d}k_z, \qquad (15)$$

$$\sigma^{S_z}_{xy,\mathrm{approx,3D}}(E) \propto \frac{1}{\langle B_{\mathrm{em},z}\rangle}\int n(E,k_z)\,\mathrm{d}k_z \qquad (16)$$

by generalizing the two-dimensional formulas from Ref. [75] in the same way as for the orbital Hall conductivity before. The result for the topological Hall conductivity is shown in Fig. 7(b) and reproduces the results of the full calculation very well; see Fig. 5(d).

Our analysis allows the understanding of the functional dependencies of the Hall conductivities presented throughout this paper. For the following discussion we consider the states with negative energy in Fig. 7. The topological Hall conductivity, shown in panel (b), characterizes charge transport. The energetically lower states are electronlike and the higher states of each block are holelike; the effective mass changes sign and the states are affected oppositely by the (emergent) magnetic field. Consequently, $\sigma_{\mathrm{approx}}(E)$ exhibits a sign change and has two extrema. However, the orbital Hall conductivity, shown in panel (a), characterizes transport of orbital angular momentum. The orbital angular momentum of a Bloch state is also dependent on the effective mass. Therefore, electronlike

and holelike states behave equally in terms of the orbital Hall transport. Consequently, $\sigma^L_{\mathrm{approx}}(E)$ does not change sign and exhibits only one extremum. By the same arguments, we can understand that the orbital Hall conductivity is an even function of the (emergent) magnetic field, while the topological Hall conductivity is odd [74,75].

IV. CONCLUSION

In summary, we have shown that a hopfion exhibits a three-dimensional topological orbital Hall effect. The emergent field itself is large within the hopfion but is compensated on a global level, which is why the charge and spin Hall conductivities are almost compensated. The square of the emergent field, however, is finite on average and causes the orbital Hall effect, which can be seen as a unique signature of the hopfion phase: Since the hopfion is an innately three-dimensional texture, it exhibits multiple tensor elements $\sigma^{L_z}_{xy}$, $\sigma^{L_x}_{yz}$, and $\sigma^{L_y}_{zx}$ (see Fig. 3), whereas a skyrmion tube, for example, is continued trivially along the tube direction and exhibits only an orbital Hall transport within the skyrmion plane.

Two-dimensional textures, such as skyrmions, are characterized by the topological charge N_{Sk} that determines their topological Hall transport. The hopfion is a three-dimensional magnetic texture that is topologically characterized by the Hopf index. Previously, the significance of this topological invariant for a hopfion's emergent electrodynamics was unknown. Here we have shown that the three-dimensional orbital Hall response of a hopfion can be seen as a signature of the Hopf index. All results presented in this paper can be interpreted based on the emergent field of the texture, which, in turn, determines its topological invariant.

Our findings present a reliable hallmark for identifying hopfions in experiments. This was difficult so far, because the commonly used real-space techniques such as LTEM penetrate the sample and result in a projected image of the texture that can hardly be distinguished from a skyrmionium. Measuring the orbital response of hopfions presents an alternative to difficult and expensive holography and tomography measurements [38–45]. Furthermore, hopfions can serve as generators of large orbital currents that can give rise to large torques, which are needed for spin-orbitronic devices.

DATA AVAILABILITY

The data that support the findings of this article are openly available [98].

[1] B. Göbel, I. Mertig, and O. A. Tretiakov, Beyond skyrmions: Review and perspectives of alternative magnetic quasiparticles, Phys. Rep. **895**, 1 (2021).

[2] A. N. Bogdanov and D. A. Yablonskii, Thermodynamically stable "vortices" in magnetically ordered crystals. The mixed state of magnets, Zh. Eksp. Teor. Fiz. **95**, 178 (1989) [Sov. Phys. JETP **68**, 101 (1989)].

[3] S. Mülbauer, B. Binz, F. Jonietz, C. Pfleiderer, A. Rosch, A. Neubauer, R. Georgii, and P. Böni, Skyrmion lattice in a chiral magnet, Science **323**, 915 (2009).

[4] X. Yu, Y. Onose, N. Kanazawa, J. Park, J. Han, Y. Matsui, N. Nagaosa, and Y. Tokura, Real-space observation of a two-dimensional skyrmion crystal, Nature (London) **465**, 901 (2010).

[5] N. Nagaosa, J. Sinova, S. Onoda, A. H. MacDonald, and N. P. Ong, Anomalous Hall effect, Rev. Mod. Phys. **82**, 1539 (2010).

[6] A. K. Nayak, V. Kumar, T. Ma, P. Werner, E. Pippel, R. Sahoo, F. Damay, U. K. Rößler, C. Felser, and S. S. Parkin, Magnetic antiskyrmions above room temperature in tetragonal Heusler materials, Nature (London) **548**, 561 (2017).

[7] L. Peng, R. Takagi, W. Koshibae, K. Shibata, K. Nakajima, T.-h. Arima, N. Nagaosa, S. Seki, X. Yu, and Y. Tokura, Controlled transformation of skyrmions and antiskyrmions in a non-centrosymmetric magnet, Nat. Nanotechnol. **15**, 181 (2020).

[8] J. Jena, B. Göbel, T. Ma, V. Kumar, R. Saha, I. Mertig, C. Felser, and S. S. Parkin, Elliptical Bloch skyrmion chiral twins in an antiskyrmion system, Nat. Commun. **11**, 1115 (2020).

[9] Y. A. Kharkov, O. P. Sushkov, and M. Mostovoy, Bound states of skyrmions and merons near the Lifshitz point, Phys. Rev. Lett. **119**, 207201 (2017).

[10] B. Göbel, A. Mook, J. Henk, I. Mertig, and O. A. Tretiakov, Magnetic bimerons as skyrmion analogues in in-plane magnets, Phys. Rev. B **99**, 060407(R) (2019).

[11] N. Gao, S.-G. Je, M.-Y. Im, J. W. Choi, M. Yang, Q.-C. Li, T. Wang, S. Lee, H.-S. Han, K.-S. Lee et al., Creation and annihilation of topological meron pairs in in-plane magnetized films, Nat. Commun. **10**, 5603 (2019).

[12] N. Nagaosa and Y. Tokura, Topological properties and dynamics of magnetic skyrmions, Nat. Nanotechnol. **8**, 899 (2013).

[13] P. Bruno, V. K. Dugaev, and M. Taillefumier, Topological Hall effect and Berry phase in magnetic nanostructures, Phys. Rev. Lett. **93**, 096806 (2004).

[14] A. Neubauer, C. Pfleiderer, B. Binz, A. Rosch, R. Ritz, P. Niklowitz, and P. Böni, Topological Hall effect in the A phase of MnSi, Phys. Rev. Lett. **102**, 186602 (2009).

[15] M. Lee, W. Kang, Y. Onose, Y. Tokura, and N. P. Ong, Unusual Hall effect anomaly in MnSi under pressure, Phys. Rev. Lett. **102**, 186601 (2009).

[16] M. Raju, A. Petrović, A. Yagil, K. Denisov, N. Duong, B. Göbel, E. Şaşıoğlu, O. Auslaender, I. Mertig, I. Rozhansky et al., Colossal topological Hall effect at the transition between isolated and lattice-phase interfacial skyrmions, Nat. Commun. **12**, 2758 (2021).

[17] B. Göbel, A. Mook, J. Henk, and I. Mertig, Antiferromagnetic skyrmion crystals: Generation, topological Hall, and topological spin Hall effect, Phys. Rev. B **96**, 060406(R) (2017).

[18] B. Göbel, A. Mook, J. Henk, and I. Mertig, The family of topological Hall effects for electrons in skyrmion crystals, Eur. Phys. J. B **91**, 179 (2018).

[19] B. Göbel, A. Schäffer, J. Berakdar, I. Mertig, and S. Parkin, Electrical writing, deleting, reading, and moving of magnetic skyrmioniums in a racetrack device, Sci. Rep. **9**, 12119 (2019).

[20] P. K. Sivakumar, B. Göbel, E. Lesne, A. Markou, J. Gidugu, J. M. Taylor, H. Deniz, J. Jena, C. Felser, I. Mertig et al., Topological Hall signatures of two chiral spin textures hosted in a single tetragonal inverse Heusler thin film, ACS Nano **14**, 13463 (2020).

[21] H. Hopf, Über die abbildungen der dreidimensionalen sphäre auf die kugelfläche, Math. Ann. **104**, 637 (1931).

[22] V. E. Korepin and L. D. Faddeev, Quantization of solitons, Theor. Math. Phys. **25**, 1039 (1975).

[23] P. Sutcliffe, Vortex rings in ferromagnets: Numerical simulations of the time-dependent three-dimensional Landau-Lifshitz equation, Phys. Rev. B **76**, 184439 (2007).

[24] P. Sutcliffe, Skyrmion knots in frustrated magnets, Phys. Rev. Lett. **118**, 247203 (2017).

[25] P. Sutcliffe, Hopfions in chiral magnets, J. Phys. A: Math. Theor. **51**, 375401 (2018).

[26] Y. Liu, R. K. Lake, and J. Zang, Binding a hopfion in a chiral magnet nanodisk, Phys. Rev. B **98**, 174437 (2018).

[27] J.-S. B. Tai, I. I. Smalyukh et al., Static Hopf solitons and knotted emergent fields in solid-state noncentrosymmetric magnetic nanostructures, Phys. Rev. Lett. **121**, 187201 (2018).

[28] X. S. Wang, A. Qaiumzadeh, and A. Brataas, Current-driven dynamics of magnetic hopfions, Phys. Rev. Lett. **123**, 147203 (2019).

[29] B. Göbel, C. A. Akosa, G. Tatara, and I. Mertig, Topological Hall signatures of magnetic hopfions, Phys. Rev. Res. **2**, 013315 (2020).

[30] Y. Liu, W. Hou, X. Han, and J. Zang, Three-dimensional dynamics of a magnetic hopfion driven by spin transfer torque, Phys. Rev. Lett. **124**, 127204 (2020).

[31] D. Raftrey and P. Fischer, Field-driven dynamics of magnetic hopfions, Phys. Rev. Lett. **127**, 257201 (2021).

[32] N. Kent, N. Reynolds, D. Raftrey, I. T. Campbell, S. Virasawmy, S. Dhuey, R. V. Chopdekar, A. Hierro-Rodriguez, A. Sorrentino, E. Pereiro et al., Creation and observation of hopfions in magnetic multilayer systems, Nat. Commun. **12**, 1562 (2021).

[33] F. N. Rybakov, N. S. Kiselev, A. B. Borisov, L. Döring, C. Melcher, and S. Blügel, Magnetic hopfions in solids, APL Mater. **10**, 111113 (2022).

[34] D. Popadiuk, E. Tartakovskaya, M. Krawczyk, and K. Guslienko, Emergent magnetic field and nonzero gyrovector of the toroidal magnetic hopfion, Phys. Status Solidi Rapid Res. Lett. **17**, 2300131 (2023).

[35] F. Zheng, N. S. Kiselev, F. N. Rybakov, L. Yang, W. Shi, S. Blügel, and R. E. Dunin-Borkowski, Hopfion rings in a cubic chiral magnet, Nature (London) **623**, 718 (2023).

[36] X. Zhang, J. Xia, Y. Zhou, D. Wang, X. Liu, W. Zhao, and M. Ezawa, Control and manipulation of a magnetic skyrmionium in nanostructures, Phys. Rev. B **94**, 094420 (2016).

[37] S. Zhang, F. Kronast, G. van der Laan, and T. Hesjedal, Real-space observation of skyrmionium in a ferromagnet-magnetic topological insulator heterostructure, Nano Lett. **18**, 1057 (2018).

[38] D. Wolf, N. Biziere, S. Sturm, D. Reyes, T. Wade, T. Niermann, J. Krehl, B. Warot-Fonrose, B. Büchner, E. Snoeck et al., Holographic vector field electron tomography of three-dimensional nanomagnets, Commun. Phys. **2**, 87 (2019).

[39] P. A. Midgley and R. E. Dunin-Borkowski, Electron tomography and holography in materials science, Nat. Mater. **8**, 271 (2009).

[40] A. Hierro-Rodriguez, C. Quirós, A. Sorrentino, L. M. Álvarez-Prado, J. I. Martín, J. M. Alameda, S. McVitie, E. Pereiro, M. Velez, and S. Ferrer, Revealing 3D magnetization of thin films with soft x-ray tomography: Magnetic singularities and topological charges, Nat. Commun. **11**, 6382 (2020).

[41] D. Wolf, S. Schneider, U. K. Rößler, A. Kovács, M. Schmidt, R. E. Dunin-Borkowski, B. Büchner, B. Rellinghaus, and A. Lubk, Unveiling the three-dimensional magnetic texture of skyrmion tubes, Nat. Nanotechnol. **17**, 250 (2022).

[42] S. Seki, M. Suzuki, M. Ishibashi, R. Takagi, N. Khanh, Y. Shiota, K. Shibata, W. Koshibae, Y. Tokura, and T. Ono, Direct visualization of the three-dimensional shape of skyrmion strings in a noncentrosymmetric magnet, Nat. Mater. **21**, 181 (2022).

[43] F. S. Yasin, J. Masell, Y. Takahashi, T. Akashi, N. Baba, K. Karube, D. Shindo, T. Arima, Y. Taguchi, Y. Tokura *et al.*, Bloch point quadrupole constituting hybrid topological strings revealed with electron holographic vector field tomography, Adv. Mater. **36**, 2311737 (2024).

[44] M. Winterott and S. Lounis, Unlocking hidden potential in electron holography of non-collinear spin textures, arXiv:2502.18949.

[45] G. Gubbiotti, A. Barman, S. Ladak, C. Bran, D. Grundler, M. Huth, H. Plank, G. Schmidt, S. Van Dijken, R. Streubel *et al.*, 2025 roadmap on 3D nano-magnetism, J. Phys.: Condens. Matter **37**, 143502 (2025).

[46] L. S. Levitov, Y. V. Nazarov, and G. M. Éliashberg, Magneto-electric effects in conductors with mirror isomer symmetry, Sov. Phys. JETP **61**, 133 (1985).

[47] T. Yoda, T. Yokoyama, and S. Murakami, Current-induced orbital and spin magnetizations in crystals with helical structure, Sci. Rep. **5**, 12024 (2015).

[48] T. Yoda, T. Yokoyama, and S. Murakami, Orbital Edelstein effect as a condensed-matter analog of solenoids, Nano Lett. **18**, 916 (2018).

[49] D. Go, J.-P. Hanke, P. M. Buhl, F. Freimuth, G. Bihlmayer, H.-W. Lee, Y. Mokrousov, and S. Blügel, Toward surface orbitronics: Giant orbital magnetism from the orbital Rashba effect at the surface of *sp*-metals, Sci. Rep. **7**, 46742 (2017).

[50] L. Salemi, M. Berritta, A. K. Nandy, and P. M. Oppeneer, Orbitally dominated Rashba-Edelstein effect in noncentrosymmetric antiferromagnets, Nat. Commun. **10**, 5381 (2019).

[51] A. Johansson, B. Göbel, J. Henk, M. Bibes, and I. Mertig, Spin and orbital Edelstein effects in a two-dimensional electron gas: Theory and application to SrTiO$_3$ interfaces, Phys. Rev. Res. **3**, 013275 (2021).

[52] Y. Liu, J. Xiao, J. Koo, and B. Yan, Chirality-driven topological electronic structure of DNA-like materials, Nat. Mater. **20**, 638 (2021).

[53] B. Kim, D. Shin, S. Namgung, N. Park, K.-W. Kim, and J. Kim, Optoelectronic manifestation of orbital angular momentum driven by chiral hopping in helical Se chains, ACS Nano **17**, 18873 (2023).

[54] A. El Hamdi, J.-Y. Chauleau, M. Boselli, C. Thibault, C. Gorini, A. Smogunov, C. Barreteau, S. Gariglio, J.-M. Triscone, and M. Viret, Observation of the orbital inverse Rashba–Edelstein effect, Nat. Phys. **19**, 1855 (2023).

[55] K. Hagiwara, Y.-J. Chen, D. Go, X. L. Tan, S. Grytsiuk, K.-H. O. Yang, G.-J. Shu, J. Chien, Y.-H. Shen, X.-L. Huang *et al.*, Orbital topology of chiral crystals for orbitronics, Adv. Mater. **37**, 2418040 (2025).

[56] J. M. Lee, M. J. Park, and H.-W. Lee, Orbital Edelstein effect of electronic itinerant orbital motion at edges, Phys. Rev. B **110**, 134436 (2024).

[57] B. Göbel, L. Schimpf, and I. Mertig, Chirality-induced orbital Edelstein effect in an analytically solvable model, Phys. Rev. Res. **7**, 033180 (2025).

[58] O. Busch, F. Ziolkowski, B. Göbel, I. Mertig, and J. Henk, Nonlinear spin and orbital Rashba-Edelstein effects induced by a femtosecond laser pulse Simulations for Au(001), Phys. Rev. Res. **7**, 043023 (2025).

[59] B. Göbel, I. Mertig, and S. Lounis, Chirality-induced selectivity of angular momentum by orbital Edelstein effect in carbon nanotubes, Commun. Phys. **8**, 395 (2025).

[60] S. Zhang and Z. Yang, Intrinsic spin and orbital angular momentum Hall effect, Phys. Rev. Lett. **94**, 066602 (2005).

[61] B. A. Bernevig, T. L. Hughes, and S.-C. Zhang, Orbitronics: The intrinsic orbital current in *p*-doped silicon, Phys. Rev. Lett. **95**, 066601 (2005).

[62] H. Kontani, T. Tanaka, D. S. Hirashima, K. Yamada, and J. Inoue, Giant intrinsic spin and orbital Hall effects in Sr$_2$$MO_4$ (M = Ru, Rh, Mo), Phys. Rev. Lett. **100**, 096601 (2008).

[63] T. Tanaka, H. Kontani, M. Naito, T. Naito, D. S. Hirashima, K. Yamada, and J. Inoue, Intrinsic spin Hall effect and orbital Hall effect in 4*d* and 5*d* transition metals, Phys. Rev. B **77**, 165117 (2008).

[64] H. Kontani, T. Tanaka, D. S. Hirashima, K. Yamada, and J. Inoue, Giant orbital Hall effect in transition metals: Origin of large spin and anomalous Hall effects, Phys. Rev. Lett. **102**, 016601 (2009).

[65] D. Go, D. Jo, C. Kim, and H.-W. Lee, Intrinsic spin and orbital Hall effects from orbital texture, Phys. Rev. Lett. **121**, 086602 (2018).

[66] A. Pezo, D. Garcia Ovalle, and A. Manchon, Orbital Hall effect in crystals: Interatomic versus intra-atomic contributions, Phys. Rev. B **106**, 104414 (2022).

[67] L. M. Canonico, T. P. Cysne, A. Molina-Sanchez, R. B. Muniz, and T. G. Rappoport, Orbital Hall insulating phase in transition metal dichalcogenide monolayers, Phys. Rev. B **101**, 161409(R) (2020).

[68] T. P. Cysne, S. Bhowal, G. Vignale, and T. G. Rappoport, Orbital Hall effect in bilayer transition metal dichalcogenides: From the intra-atomic approximation to the Bloch states orbital magnetic moment approach, Phys. Rev. B **105**, 195421 (2022).

[69] L. Salemi and P. M. Oppeneer, Theory of magnetic spin and orbital Hall and Nernst effects in bulk ferromagnets, Phys. Rev. B **106**, 024410 (2022).

[70] O. Busch, I. Mertig, and B. Göbel, Orbital Hall effect and orbital edge states caused by *s* electrons, Phys. Rev. Res. **5**, 043052 (2023).

[71] Y.-G. Choi, D. Jo, K.-H. Ko, D. Go, K.-H. Kim, H. G. Park, C. Kim, B.-C. Min, G.-M. Choi, and H.-W. Lee, Observation of the orbital Hall effect in a light metal Ti, Nature (London) **619**, 52 (2023).

[72] I. Lyalin, S. Alikhah, M. Berritta, P. M. Oppeneer, and R. K. Kawakami, Magneto-optical detection of the orbital Hall effect in chromium, Phys. Rev. Lett. **131**, 156702 (2023).

[73] O. Busch, F. Ziolkowski, B. Göbel, I. Mertig, and J. Henk, Ultrafast orbital Hall effect in metallic nanoribbons, Phys. Rev. Res. **6**, 013208 (2024).

[74] B. Göbel and I. Mertig, Orbital Hall effect accompanying quantum Hall effect: Landau levels cause orbital polarized edge currents, Phys. Rev. Lett. **133**, 146301 (2024).

[75] B. Göbel, L. Schimpf, and I. Mertig, Topological orbital Hall effect caused by skyrmions and antiferromagnetic skyrmions, Commun. Phys. **8**, 17 (2025).

[76] M. d. S. Dias, J. Bouaziz, M. Bouhassoune, S. Blügel, and S. Lounis, Chirality-driven orbital magnetic moments as a new probe for topological magnetic structures, Nat. Commun. **7**, 13613 (2016).

[77] F. R. Lux, F. Freimuth, S. Blügel, and Y. Mokrousov, Engineering chiral and topological orbital magnetism of domain walls and skyrmions, Commun. Phys. **1**, 60 (2018).

[78] B. Göbel, A. Mook, J. Henk, and I. Mertig, Magnetoelectric effect and orbital magnetization in skyrmion crystals: Detection and characterization of skyrmions, Phys. Rev. B **99**, 060406(R) (2019).

[79] J. Barker and O. A. Tretiakov, Static and dynamical properties of antiferromagnetic skyrmions in the presence of applied current and temperature, Phys. Rev. Lett. **116**, 147203 (2016).

[80] X. Zhang, Y. Zhou, and M. Ezawa, Magnetic bilayer-skyrmions without skyrmion Hall effect, Nat. Commun. **7**, 10293 (2016).

[81] X. Zhang, Y. Zhou, and M. Ezawa, Antiferromagnetic skyrmion: Stability, creation and manipulation, Sci. Rep. **6**, 24795 (2016).

[82] W. Legrand, D. Maccariello, F. Ajejas, S. Collin, A. Vecchiola, K. Bouzehouane, N. Reyren, V. Cros, and A. Fert, Room-temperature stabilization of antiferromagnetic skyrmions in synthetic antiferromagnets, Nat. Mater. **19**, 34 (2020).

[83] J. Whitehead, An expression of Hopf's invariant as an integral, Proc. Natl. Acad. Sci. USA **33**, 117 (1947).

[84] F. Wilczek and A. Zee, Linking numbers, spin, and statistics of solitons, Phys. Rev. Lett. **51**, 2250 (1983).

[85] R. Knapman, M. Azhar, A. Pignedoli, L. Gallard, R. Hertel, J. Leliaert, and K. Everschor-Sitte, Numerical calculation of the Hopf index for three-dimensional magnetic textures, Phys. Rev. B **111**, 134408 (2025).

[86] K. Ohgushi, S. Murakami, and N. Nagaosa, Spin anisotropy and quantum Hall effect in the kagomé lattice: Chiral spin state based on a ferromagnet, Phys. Rev. B **62**, R6065 (2000).

[87] K. Hamamoto, M. Ezawa, and N. Nagaosa, Quantized topological Hall effect in skyrmion crystal, Phys. Rev. B **92**, 115417 (2015).

[88] B. Göbel, A. Mook, J. Henk, and I. Mertig, Unconventional topological Hall effect in skyrmion crystals caused by the topology of the lattice, Phys. Rev. B **95**, 094413 (2017).

[89] G. Yin, Y. Liu, Y. Barlas, J. Zang, and R. K. Lake, Topological spin Hall effect resulting from magnetic skyrmions, Phys. Rev. B **92**, 024411 (2015).

[90] M.-C. Chang and Q. Niu, Berry phase, hyperorbits, and the Hofstadter spectrum: Semiclassical dynamics in magnetic Bloch bands, Phys. Rev. B **53**, 7010 (1996).

[91] P. Oppeneer, Magneto-optical spectroscopy in the valence-band energy regime: Relationship to the magnetocrystalline anisotropy, J. Magn. Magn. Mater. **188**, 275 (1998).

[92] D. Xiao, J. Shi, and Q. Niu, Berry phase correction to electron density of states in solids, Phys. Rev. Lett. **95**, 137204 (2005).

[93] T. Thonhauser, D. Ceresoli, D. Vanderbilt, and R. Resta, Orbital magnetization in periodic insulators, Phys. Rev. Lett. **95**, 137205 (2005).

[94] D. Ceresoli, T. Thonhauser, D. Vanderbilt, and R. Resta, Orbital magnetization in crystalline solids: Multi-band insulators, Chern insulators, and metals, Phys. Rev. B **74**, 024408 (2006).

[95] A. Raoux, F. Piéchon, J.-N. Fuchs, and G. Montambaux, Orbital magnetism in coupled-bands models, Phys. Rev. B **91**, 085120 (2015).

[96] B. Göbel, A. Mook, J. Henk, and I. Mertig, Signatures of lattice geometry in quantum and topological Hall effect, New J. Phys. **19**, 063042 (2017).

[97] L. Onsager, Interpretation of the de Haas–van Alphen effect, London Edinburgh Dublin Philos. Mag. J. Sci. **43**, 1006 (1952).

[98] Data are provided for figures shown in this paper at Zenodo (2025), doi: 10.5281/zenodo.15609600.